

# VARIATIONAL GAUSSIAN PROCESS FOR OPTIMAL SENSOR PLACEMENT

GABOR TAJNAFOI, London, ROSSELLA ARCUCCI, London, LAETITIA MOTTET,  
London, CAROLANNE VOURIOT, London, MIGUEL MOLINA-SOLANA, Granada,  
CHRISTOPHER PAIN, London, YI-KE GUO, London

(Received November 15, 2019)

*Abstract.* Sensor placement is an optimisation problem that has recently gained great relevance. In order to achieve accurate online updates of a predictive model, sensors are used to provide observations. When sensors location is optimally selected, the predictive model can greatly reduce its internal errors. A greedy-selection algorithm is used for locating these optimal spatial locations from a numerical embedded space. A novel architecture for solving this big data problem is proposed, relying on a Variational Gaussian Process. The generalisation of the model is further improved via the preconditioning of its inputs: Masked Autoregressive Flows are implemented to learn non-linear, invertible transformations of the conditionally modelled spatial features. Finally, a global optimisation strategy extending the Mutual Information-based optimisation and fine-tuning of the selected optimal location is proposed. The methodology is parallelised to speed-up the computational time, making these tools very fast despite the high complexity associated with both spatial modelling and placement tasks. The model is applied to a real three-dimensional test case considering a room within the Clarence Centre building located in Elephant and Castle, London, UK.

*Keywords:* Sensor placement, Variational Gaussian Processes, Mutual Information

*MSC 2010:* 65Z05, 68T99

## 1. INTRODUCTION

1

2 Indoor Air Quality (IAQ) impacts health, comfort and quality of life [1], and three  
3 basic strategies have been proposed to improve it: control of pollution sources, use  
4 of natural/mechanical ventilation, and cleaning of air. In the building context, the  
5 management and development of smart monitoring tools can support an adequate

6 IAQ within them (e.g. by automatically opening windows or starting a mechanical  
7 air cleaning system). Sensors coupled with indoor pollutant forecasting models can  
8 tackle bad IAQ by implementing one of the previously-cited strategies before the  
9 indoor pollutant concentration reaches dangerous and adverse levels.

10 In order to achieve accurate, online updates of the predictive model, sensors can  
11 be used to provide observations. Spatio-temporal models such as Data Assimilation  
12 (DA) provide online learning and forecasting of sensor observations by means of  
13 updating the model’s internal view through the incorporation of collected data [2, 3].  
14 In this context, sensor positioning has gained relevance [4, 5] as it is crucial to ensure a  
15 good quality and usefulness of monitored data. Optimal sensor positioning tools pin-  
16 point the discrete spatial locations that possess most conditional information of all  
17 other spatial points, thus improving the predictive accuracy of prediction models [6].  
18 Hence, sensor placement can be seen as an optimisation problem [4, 5].

19 Early attempts on sensor placement used geometric approaches, supported by the  
20 assumption that sensors measure spatial features with a fixed sensing radius [7]. This  
21 geometric approach does not take into account the non-linear dynamic behaviour of  
22 air motion so, in order to tackle this problem, parametric models [8], non-parametric  
23 Gaussian Process (GP) [9] and ensemble Kalman-filters [10] approaches were subse-  
24 quently proposed.

25 The main work on this field implements sensor placement using a GP in a 2D space  
26 [5]. The time complexity of the placement algorithm is  $O(N^4)$ , where  $N$  denotes the  
27 side of the computational domain. The GP is trained on data collected from fixed  
28 sensors located in a room, then  $N$  is relatively small. The placement algorithm only  
29 select the best sensors in the set already provided.

30 In this work, for the first time, a sensor placement model is developed for a 3D  
31 domain representing a real case scenario. Also, the model uses temporal sequences  
32 of data from fluid dynamic simulations facing then a big data problem. In our  
33 case,  $N$  is on an scale such that the use of a GP is unfeasible. To address this  
34 problem we developed a combination of deep learning, probabilistic frameworks and  
35 variational methods, reducing the complexity associated with training, inference and  
36 optimisation and thus, enabling us to achieve optimal placement results in a real case  
37 scenario. The complexity of our model is, in fact,  $O(klM^4)$ , where  $k$  is the number  
38 of sensors,  $l$  is the number of iteration needed to optimise the position and  $M$  is such  
39 that  $M \ll N$ .

40 The rest of this paper is organized as follows: next section introduces the back-  
41 ground to this work and our main contributions. Section 3 presents the mathemati-  
42 cal formulation of our proposed model, Variational Gaussian Process optimal sensor  
43 placement (VGPosp). Section 4 describes the direct application of VGPosp on a real  
44 indoor environment. The manuscript ends with some conclusions and further work.

## 45 2. BACKGROUND AND MAIN CONTRIBUTIONS

46 Non-parametric models consist in learning a Gaussian Process (GP) associated with  
47 the phenomenology considered (e.g. pollution levels in indoor environments). In  
48 general, GPs are highly appropriate to study environmental problems as they allow  
49 for learning complex, high-dimensional correlations with uncertainty quantification.  
50 Indeed, non-parametric expressiveness is an advantage over parametric models that  
51 are more prone to the curse of dimensionality [11]. A GP, sometimes referred as  
52 the Bayesian interpretation of neural networks, is fully determined by only two pa-  
53 rameters, namely the mean-function and covariance-function, regardless of their di-  
54 mensionality [12]. Three main GP methodologies can be identified: the Traditional  
55 GP [4, 5], the Sparse GP [13] and the Variational GP [14, 15].

56 Traditional GP is a stochastic process based on prior distribution over functions and  
57 it has been successfully applied for indoor optimal sensor positioning [4, 5]. However,  
58 Traditional GP suffers from the high complexities associated with spatial modelling  
59  $O((mN)^3)$ , where  $N$  denotes the size of input sensor potential locations and  $m$  the  
60 number of physical variables, which explains why the work presented in [4, 5] was  
61 only carried out in two dimensions.

62 Sparse Variational Process (SGP) tackles the inconvenient  $O((mN)^3)$  computational  
63 complexity associated with Traditional GP [16]. This method constructs an approx-  
64 imation based on a small subset of size  $\hat{N}$ , namely inducing points. This optimisa-  
65 tion results in a reduced complexity  $O((mN)\hat{N}^2)$ , enabling the scalability of training  
66 data-points from the previous limit of a few thousand to the range of millions [17].  
67 In general, sparsity can be achieved by working on a low-rank representation of the  
68 full kernel [18]. The key idea is to approximate the prior or modify the likelihood  
69 function, thus creating a model selection problem solving the optimisation for the  
70 approximation of the truth [13]. However, the main criticism to SGPs is that they  
71 learn unknown hyperparameters, potentially leading them to underestimate variance  
72 and thus over-fitting [14, 15].

73 Alternatively, Variational Gaussian Process (VGP), a variational method for SGP,  
74 was developed [14, 15] to deal with the approximation of model components that

75 are hard to compute. Inducing points are variational parameters selected by min-  
76 imising the Kullback-Leibler (KL) divergence [14, 15]. The kernel hyperparameters  
77 and inducing points are jointly optimised by maximising a lower bound (Evidence  
78 Lower BOund (ELBO)) of variational distribution over the functions latent val-  
79 ues [14, 15, 19]. The key innovation, is that the likelihood and the GP prior are  
80 not modified, separating the model and the inference. The variational posterior  
81 iteratively approaches the true posterior.

82 The datasets used to train a GP usually comprises data coming from monitoring  
83 sensors during extensive field experiment periods. This training dataset usually suffer  
84 from being non-Gaussian distributed, rendering it unusable for GP learning [20]. In  
85 this regards, several methodologies to precondition, normalise and render the training  
86 dataset Gaussian can be mentioned: Variational Autoencoder [21], Autoregressive  
87 Flows [22], Normalising Flows [23], Masked Autoencoder for Distribution Estimation  
88 (MADE) [24], and Masked Autoregressive Flows (MAF) [20]. The MAF approach  
89 is a stack of MADE networks [24, 20] and has proved its competitiveness over the  
90 other methodologies in terms of accuracy [20].

91 Even if VGP can deal with non-Gaussian distributed data, the preconditioning phase  
92 of learning non-linear, invertible transformations between the conditional input dis-  
93 tributions and output Gaussian family of distributions enables greater generalisation  
94 of the learned spatial model.

95 At this stage, the actual sensors placement problem can then be addressed using  
96 the trained GP. Indeed, the placement algorithm is solved in an embedded space  
97 that is predicted by a GP [14, 15]. In other words, the GP serves as a numerical  
98 setting for the optimisation problem: conditional predictions are used to generate  
99 the covariance matrix taken as input by the placement algorithm. The complexity  
100 associated with the placement task is  $O(N^4)$ , where  $N$  denotes the size of input  
101 sensor potential locations.

102 Mutual Information (MI) [4, 5] and minimum cross entropy [25, 26] are some of the  
103 metrics traditionally used. The use of minimum cross entropy tends to maximise the  
104 distance between sensors. In indoor environment problems, this results in having  
105 sensors located near the boundary of the domain, i.e. near the walls, thus loosing  
106 information monitored [26, 5]. One the other hand, information gain or Mutual  
107 Information [4] shifts the amount of information captured by a single random variable  
108 to the information each random variable has of the other unobserved one. More  
109 specifically, considering a finite set of possible placement locations, by maximising  
110 the objective metric, it evaluates how well a given smaller subset of sensor locations  
111 describes the values of the unselected other locations. This paper considers the

112 optimisation problem of sensor placement in indoor environments by separating the  
113 problem into the learning of a spatial model, i.e. Gaussian Process training, and  
114 the optimisation algorithm itself, i.e. optimal sensor placement. It is demonstrated  
115 that with a combination of deep learning, probabilistic frameworks and variational  
116 methods, the complexity associated with training, inference and optimisation can be  
117 significantly reduced in order to achieve optimal placement results. This paper builds  
118 on existing 2D sensor placement algorithm [4, 5] and the latest VGP spatial modelling  
119 technologies [14, 15]. Its value is found primarily in the pairing of technologies that  
120 in turn improve the existing methods of sensor placement.

121 The choice of the technologies used in this work are detailed and argued in the  
122 following points:

- 123 • **Preprocessing input distribution** A Masked Autoregressive Flow (MAF)  
124 is used to normalise the training dataset suffering from being non-Gaussian  
125 distributed [20] making our methodology greatly generalised as well as im-  
126 proving the accuracy.
  
- 127 • **Spatial model** A major challenge facing scalable sensor placement is over-  
128 come by deploying a Variational Gaussian Process (VGP), using a low  
129 rank approximation that is far more scalable and also addresses the ques-  
130 tion of model generalisation. In particular, this helps to tackle the limit-  
131 ing  $O((mN)^3)$ , high polynomial time complexities associated with GPs to  
132  $O((mN)\hat{N}^2)$  where  $\hat{N}$  denotes the number of approximate posterior samples  
133 computed in the VGP. Using a VGP is a good trade-off between efficiency  
134 and accuracy [14, 15].
  
- 135 • **Sensor placement algorithm** The Mutual Information (MI) based place-  
136 ment algorithm [4, 5] is extended with a Markov-Chain Monte Carlo (MCMC)  
137 wrapper to fine-tune the sensor placement and tackle the time complexity  
138  $O(N^4)$  and achieve  $O(klM^4)$ , where  $k$  is the number of sensors,  $l$  is the num-  
139 ber of iteration needed to optimise the position and  $M$  is such that  $M \ll N$ .  
140 The use of MCMC leads to similar placement results in a fraction of the  
141 computation time required when not using it. Error propagation through  
142 the system does exist due to this approximation, however, it is shown in the  
143 paper to be a worthwhile trade-off.

144 The technologies used in this paper are general and are not limited to the test case  
145 of sensor placement in indoor environments, even though their integrated implemen-  
146 tation was designed accordingly. In fact, the core underlying technology used in the

147 spatial model, i.e. Variational Gaussian Process, has been successfully deployed for  
148 a multitude of other domains ranging from kriging to robotics [27].

149 In addition to the new pairing of technologies proposed in this paper, the novelties  
150 of this work also lie in:

- 151 • **The simulated training data** In order to achieve scalable and reduced cost  
152 deployment of sensor placement optimisation, simulation data was used for  
153 model training, replacing the expensive option of collecting large amounts  
154 measurements from installed sensors. As an example, the training dataset  
155 used in [5] consists of 52 sensors, located on a 2D plan. In this paper, the  
156 simulated training dataset is much larger, i.e. more reliable, and consist of  
157 10,000 sensor locations distributed in 3D.
- 158 • **The increase in dimensionality** This paper increases the dimensionality of  
159 the learning problem in order to capture further correlations between hidden  
160 features as well as the output features, resulting in 3-dimensional spatial  
161 placement. The 3D placement made it possible for the model to capture more  
162 realistic and complex physical phenomena such as thermal stratification for  
163 example.
- 164 • **The fine-tuning of sensor placement** The MCMC wrapper algorithm is  
165 used to increase the overall Mutual Information captured. The base set of  
166 potential sensor location is fine-tuned to include other regions in the contin-  
167 uous space having higher MI. This means the selection pipeline is a more  
168 optimal set of possible placement coordinates to choose from. Additionally,  
169 the implementation is easy to be customised and makes our methodology  
170 generalisable.
- 171 • **The fully parallel and scalable implementation** The methodology pre-  
172 sented in this paper is done through a multi-threaded parallel implementa-  
173 tion. The computational graph based implementation, using the TensorFlow  
174 library [28], greatly speeds up the computational times.

### 175 3. THE VARIATIONAL GAUSSIAN PROCESS FOR OPTIMAL SENSOR PLACEMENT 176 (VGPOSP) MODEL

177 This section introduces the theoretical concepts and mathematical formulation that  
178 were developed and implemented as part of the proposed model architecture.

179 Let  $X$  be the solution of a dynamic system:

$$(3.1) \quad \dot{X} = F(X, t)$$

180 where,  $t$  denotes the time and  $X = [X_1, \dots, X_m]$  denotes a vector of  $m$  state vari-  
 181 ables<sup>1</sup> such that  $X_i \in \mathfrak{R}^N, \forall i = 1, \dots, m$ . In the following,  $X_t = X(t)$  denotes the  
 182 solution of the dynamic system at time  $t$  and  $X_{i,t} = X_i(t)$  the  $i$ -th state variable at  
 183 time  $t$ .

184 Given a temporal sequence  $X_{t_1}, \dots, X_{t_n}$  of  $n$  solutions of the dynamical system de-  
 185 fined in equation (3.1), with  $X_{t_i} = [X_{1,t_i}, \dots, X_{m,t_i}] \forall i = 1, \dots, n$ , the Variational  
 186 Gaussian Process for optimal sensor placement (VGPosp) model consists of the fol-  
 187 lowing main steps described in the sub-sections 3.1 to 3.3.

- 188 • **Section 3.1 - Preprocessing and preconditioning**
  - 189 – Preconditioning of input vector distributions using Masked Autoregres-  
 190 sive Flows (MAF).
  - 191 – Convert time-series to vector value distributions at distinct spatial re-  
 192 gions.
- 193 • **Section 3.2 - Variational Gaussian Process**
  - 194 – Sampling algorithm, input vectors spatial training.
  - 195 – Variational Gaussian Process (VGP) training.
- 196 • **Section 3.3 - Placement algorithm**
  - 197 – Selection of a set  $S$  of considered input coordinates.
  - 198 – Generate target vectors with VGP inference at coordinates.
  - 199 – Covariance matrix of values indexed by set  $S$ .
  - 200 – Greedy selection algorithm of coordinates with maximal Mutual Infor-  
 201 mation (MI).
  - 202 – Markov-Chain Monte Carlo (MCMC) based fine-tuning of coordinates.

203 **3.1. Pre-processing and preconditioning.** The temporal sequence  $X_{t_1}, \dots, X_{t_n}$   
 204 requires a pre-processing to be suitable for the spatial model and the inference step  
 205 during the placement algorithm. The pre-processing consists of the following steps,  
 206 also described in Figure 1:

- 207 (1)  $X$  is first normalised to a mean value of 0 and standardised to achieve a  
 208 standard deviation of each feature of 1.

---

<sup>1</sup>For example, as shown in Section 4, for fluid dynamic simulations in indoor environment,  $X = [T, P, C]$ , where  $T$  is the temperature,  $P$  the pressure and  $C$  the pollutant concentration.

209 (2) Secondly, a Masked Autoregressive Flow (MAF) is implemented to learn  
 210 invertible, non-linear transformations between the non-Gaussian distributed  
 211 features and the target Gaussian family of distributions.

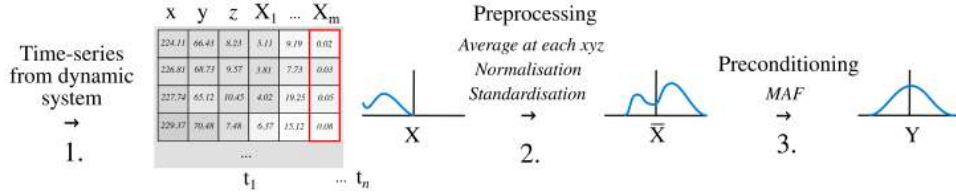


FIGURE 1. Pre-processing and pre-conditioning steps.

212 Firstly, the mean of the temporal sequence for each state variable  $X_i, i = 1, \dots, m$ ,  
 213 is computed, i.e. the vector

$$(3.2) \quad \bar{X} = [\bar{X}_1, \dots, \bar{X}_m]$$

214 where

$$(3.3) \quad \bar{X}_i = \frac{\sum_{j=1}^n X_{i,t_j}}{n}, \quad \forall i = 1, \dots, m$$

215 The vector  $\bar{X}$  in equation (3.2) is used to train the Masked Autoregressive Flows  
 216 (MAF) in order to make our input variables Gaussian distributed. MAF is a neural  
 217 network that executes a normalising flow non-linear transformation at each neuron.  
 218 MAF can be also computed as a stack of autoregressive Masked Autoencoder for  
 219 Distribution Estimation (MADE) networks [20, 24] where each model uses the vector  
 220  $\bar{X}$  in equation (3.2). The Autoregressive property of MAF defined from time-series  
 221 analysis, predicts a future value of a variable from a linear combination of its past  
 222 values. Each MADE learns the distribution of the state variables.

223 The MAF model can be defined as follows [22]:

$$(3.4) \quad \bar{X}_N = f_N(\bar{X}_{N-1}, \bar{X}_{N-2}, \dots, \bar{X}_1)$$

224 where  $f_N$  has a polynomial form such that [20]:

$$(3.5) \quad \bar{X}_N = \theta_0 + \theta_1 \bar{X}_{N-1} + \theta_2 \bar{X}_{N-2} + \dots + \theta_p \bar{X}_{N-p}$$

225 where  $\theta_i$  are the polynomial coefficients.



226 Normalising flows apply a sequence of  $N$  invertible, differentiable transformation  
 227 functions  $f_N$  in  $p(\bar{X})$ . A base distribution  $p(\bar{X}')$  is specified most likely from the  
 228 family of Gaussian distributions [20], where  $p$  denotes the probability distribution.  
 229 The procedure begins with this initial distribution  $p(\bar{X}')$  [23].

$$(3.6) \quad p(\bar{X}) = p(\bar{X}') \left| \det \frac{\partial f^{-1}}{\partial \bar{X}'} \right|$$

230 A chain rule can then be applied to the conditionals of a joint distribution.

$$(3.7) \quad p(\bar{X}) = \prod_{i=1}^N p(\bar{X}_i | \bar{X}_{i-1}, \bar{X}_{i-2}, \dots, \bar{X}_1) = \prod_{i=1}^N p(\bar{X}_i | \bar{X}_{<i})$$

231 After each non-linear transformation the distribution becomes more complex. Sam-  
 232 pling from this transformed distribution is done via the flow of a straightforward  
 233 sample from the original  $p(\bar{X})$  Gaussian distribution through the non-linear trans-  
 234 formations. The entropy of the resultant distribution is computed with the logarithm  
 235 of the transformations:

$$(3.8) \quad \log p(\bar{X}_N) = \ln p(\bar{X}_0) - \sum_{i=1}^N \ln \left| \det \frac{\partial f_N}{\partial \bar{X}_{i-1}} \right|$$

236

$$(3.9) \quad p(Y) = \prod_{i=1}^N \left( f_N^{-1}(Y) \right) \left| \det \frac{\partial f_N^{-1}}{\partial Y} \right|$$

237 The vector

$$(3.10) \quad Y = [Y_1, \dots, Y_m] \in \mathfrak{R}^{m \times N}, \quad \text{with } Y_j \in \mathfrak{R}^N \forall j = 1, \dots, m$$

238 is the set of normalised state variables which are input of the Variational Gaussian  
 239 Process introduced in next section.

240 **3.2. VGP training and inference.** Given the data set  $\{Y_j\}_{j=1}^m$  of  $Y_j \in \mathfrak{R}^N$  as  
 241 defined in equation (3.10), the  $m$  source-target pairs  $\mathcal{D} = \{(Y_j, T)\}_{j=1}^m$ , where  $T$  is a  
 242 target<sup>2</sup> [29]. We aim to learn a function over all source-target pairs:

$$(3.11) \quad T = g(Y_j)$$

---

<sup>2</sup>In some application,  $T = Y_j$  for a fixed  $j$  can be assumed.

243 where  $g : \mathbb{R}^N \rightarrow \mathbb{R}^N$  is unknown. Let the function  $g$  decouple as  $g = (g_1, \dots, g_N)$ ,  
 244 where each  $g_i : \mathbb{R}^N \rightarrow \mathbb{R}$ . A GP regression [12] estimates the functional form of  $g$  by  
 245 placing a prior,

$$(3.12) \quad p(g) = \prod_{i=1}^N \mathcal{GP}(g_i; 0, \Sigma_{ij}),$$

246 where  $\Sigma_{ij}$  denotes a covariance evaluated over pairs of inputs  $Y_i Y_j \in \mathbb{R}^N$  [12]:

$$(3.13) \quad \Sigma_{ij} = \frac{\sum_k Y_{ik} Y_{jk}^T}{N}$$

247 A variational Gaussian process (VGP) is a Bayesian non-parametric variational  
 248 model that admits arbitrary structures to match posterior distributions. As de-  
 249 scribed in the following steps, the VGP generates approximate posterior samples  $Z$   
 250 by generating latent inputs, warping them with random non-linear mappings, and  
 251 using the warped inputs as parameters to a mean-field distribution. The random  
 252 mappings are drawn conditional on variational parameters. The VGP specifies a  
 253 generative process for posterior latent variables  $Z$ . At the first step it draws la-  
 254 tent input  $\xi \in \mathbb{R}^N : \xi \sim \mathcal{N}(0, I)$  and a non-linear mapping  $g : \mathbb{R}^N \rightarrow \mathbb{R}^N$  condi-  
 255 tioned on  $\mathcal{D} : g \sim \prod_{i=1}^N \mathcal{GP}(0, \Sigma_{\xi\xi}) | \mathcal{D}$ . Then it draws approximate posterior samples  
 256  $Z \in \text{supp}(p) : Z = (Z_1, \dots, Z_{\hat{N}}) \sim \prod_{i=1}^{\hat{N}} q(g_i(\xi))$ . Marginalising over all latent inputs  
 257 and non-linear mappings, the VGP is [29]:

$$(3.14) \quad q_{VGP}(Z; \theta, \mathcal{D}) = \iint \left[ \prod_{i=1}^{\hat{N}} q(Z_i | g_i(\xi)) \right] \left[ \prod_{i=1}^{\hat{N}} \mathcal{GP}(g_i; 0, \Sigma_{\xi\xi}) | \mathcal{D} \right] \mathcal{N}(\xi; 0, I) d\xi d\xi.$$

258 The VGP is parametrised by kernel hyperparameters  $\theta$  and variational data [29, 12].  
 259 The random function interpolates the values in the variational data, which are opti-  
 260 mised to minimise the Kullback–Leibler divergence [30]. It defines a measure between  
 261 two probability density functions:  $q_{VGP}(Z; \theta, \mathcal{D})$  and  $q^*(Z|Y)$ , where  $q^*(Z|Y)$  is the  
 262 posterior distribution [31].

$$(3.15) \quad D_{KL}(q_{VGP}(Z; \theta, \mathcal{D}) || q^*(Z|Y)) = \mathbb{E}_q \left[ \log \frac{q_{VGP}(Z; \theta, \mathcal{D})}{q^*(Z|Y)} \right]$$

$$= \mathbb{E}_q \left[ \log q_{VGP}(Z; \theta, \mathcal{D}) - \log q^*(Z|Y) \right]$$

263 where [19]  $\mathbb{E}[f(x, \theta)] = \int_{\theta} f(x, \theta) d\theta$ , where  $f$  denotes a distribution function. An  
 264 approximating distribution is chosen from a predefined family of distributions with

265 parameters:  $\theta$ .

$$(3.16) \quad q_\theta(Z|Y) = \operatorname{argmin}_\theta D_{KL}(q_{VGP}(Z; \theta, \mathcal{D}) || q^*(Z|Y))$$

266 When the KL-divergence converges to 0 (see the Theorem of the Universal approx-  
 267 imation in [29]), the posterior is approximately the same as the learned posterior.  
 268 Minimising KL-divergence is done via the objective function, defined by the Evidence  
 269 Lower Bound (ELBO), parameterised by the parameters  $\theta$ . The maximisation of this  
 270 function is equivalent as minimising KL with a difference measured by a constant  
 271 factor [23]. The objective is summed over all data-points [19]:

$$(3.17) \quad \text{ELBO}(\theta) = \sum_{i=1}^{\hat{N}} \mathbb{E}_{q_\theta(Z|X_i)} [\log q_{VGP}(Z; C, Y_i) - \log q_\theta(Z|Y_i)]$$

272 When applied to the marginal probability of the evidence [29, 15], the objective lower  
 273 bound on the marginal likelihood can be quantified by the ELBO:

$$(3.18) \quad \text{ELBO}(\theta) = \mathbb{E}_q[\log q_{VGP}(Z; \theta, X)] - \mathbb{E}_q[\log q_\theta(z|x)]$$

274 Posterior is therefore the sum of the ELBO and the KL term:

$$(3.19) \quad \log q(Z) = \text{ELBO}(\theta) + D_{KL}(q_\theta(Z|Y) || q^*(Z|Y)).$$

275 An approximate solution in the mean-field [32] is sought to learn parameters of the  
 276 marginal likelihood [33], obtaining an approximate posterior distribution of the true  
 277 posterior. The mean-field approximation of variational inference allowed for the  
 278 approximate  $q_\theta(Z|Y)$  distribution to be considered as a factor of  $\hat{N}$  independent  
 279 latent variable partitions  $q_\theta(Z|Y_i)$ .

$$(3.20) \quad q^*(Z|Y) \approx q_\theta(Z|Y) = \prod_{i=1}^{\hat{N}} q_\theta(Z|Y_i)$$

280 then it yields  $g \sim q^*(Z|Y)$  [34].

281 **3.3. Placement Algorithm.** In this section, the Placement algorithm of VGPosp  
 282 model is introduced. The algorithm computes optimal coordinates for sensor place-  
 283 ment following three main steps as described in Figure 2 and detailed in Algorithm 1.

The set of coordinates  $\mathcal{V}$  initially consists of  $N$  grid point:  $|\mathcal{V}| = N$ . Our place-  
 ment algorithm is mainly based on the Mutual Information (MI) based placement  
 algorithm [4, 5] which is extended in this paper with a MCMC wrapper to fine-tune

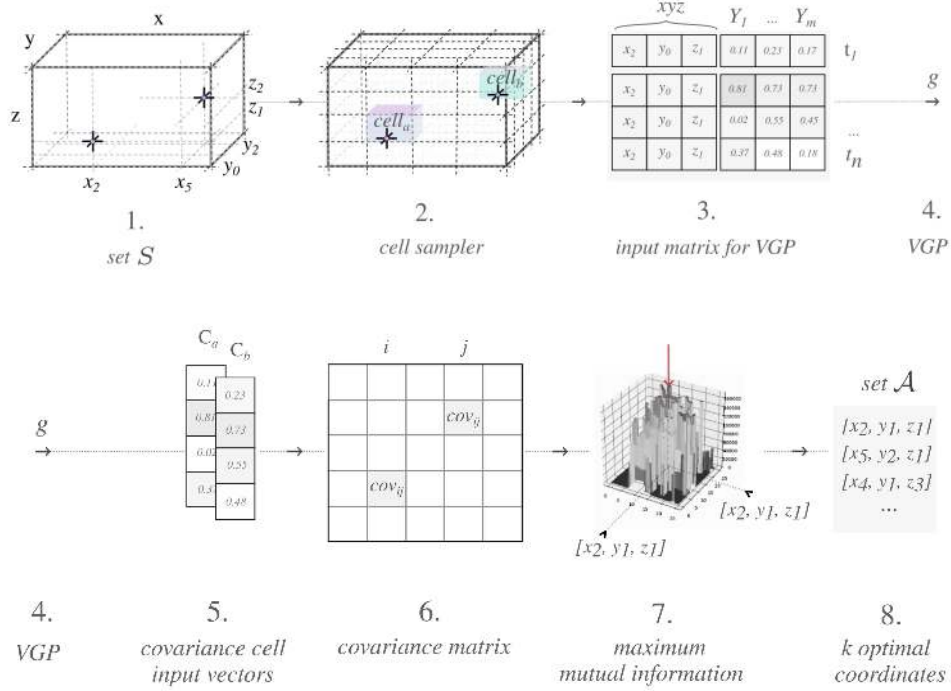


FIGURE 2. Graphical representation of the main steps of the Variational Gaussian Process for optimal sensor placement (VGPosp) model

the sensor placement and tackle the time complexity  $O(N^4)$  and achieve  $O(klM^4)$ , where  $k$  is the number of sensors,  $l$  is the number of iteration needed to optimise the position and  $M$  is a predefined small subset of  $N$  such that  $M \ll N$ . In fact, the first step of Algorithm 1 consists of identifying all the possible locations which constitutes a set  $S$ ,  $|S| = M$  (see points 1 and 2 in Figure 2). The set  $S$  is an input of Algorithm 1. Other inputs are the number  $k$  of sensors to place and the number  $l$  of maximum iterations for the optimisation process. We implement an optimisation method to identify a set  $\mathcal{A}$  as the placement output from the predefined set  $S$  of input coordinates [4] such that  $|\mathcal{A}| = k$ . The second step of Algorithm 1 consists in sampling  $m$  state variables from value distributions in  $Y$  at corresponding spatial regions/cells (see point 3 in Figure 2). For each state variable in  $Y$  (see point 4 in Figure 2), the samples  $T$  are produced by the function  $g$  which is computed by a

---

**Algorithm 1:** The Variational Gaussian Process for optimal sensor placement (VGPosp) algorithm.

---

**Input:** number of sensors:  $k$ , space of coordinates:  $S$ , maximum number of iterations:  $l$ ;  $\epsilon$

```

1  $\mathcal{A}^* = \emptyset$                                 ▷ initialise the set of optimal sensors locations
2  $\Sigma = \emptyset$                                 ▷ initialise the covariance matrix
3  $\delta_{\bar{y}} = 0$                                     ▷ initialise the mutual information parameter
4 while  $ii < k$  do
5   while  $it < l$  do                                ▷ compute the covariance matrix
6   for  $i \in S$  do
7     for  $t_k \in [t_0, t_n]$  do
8        $T_{ik} = g(Y_{ik})$                                 ▷ VGP function in 3.11
9        $T_i = [T_{i0}, T_{i1}, \dots, T_{in}]$ 
10    for  $j \in S$  do
11      for  $t_k \in [t_0, t_n]$  do
12         $T_{jk} = g(Y_{jk})$                                 ▷ VGP function in 3.11
13         $T_j = [T_{j0}, T_{j1}, \dots, T_{jn}]$ 
14      compute  $\Sigma_{ij}$                                 ▷ using equation (3.13)
15     $\mathcal{A}, \delta_{i^*} \leftarrow \text{Algorithm 2}(\Sigma, S, k)$     ▷ estimate the mutual information
16    if  $\delta_{i^*} > \delta_{\bar{y}}$  or  $\mathcal{A}^* = \emptyset$  then
17       $\mathcal{A}^* = \mathcal{A}$ 
18       $\delta_{\bar{y}} = \delta_{i^*}$ 
19     $it++$ 
20   $ii++$ 
21 return  $\mathcal{A}^*$ 

```

---

VGP as described in section 3.2 (see points 9-14 in Algorithm 1):

$$\forall j \in S, \quad T_{jk} = g(Y_{jk}), \quad T_j = [T_{j0}, T_{j1}, \dots, T_{jn}]$$

284 Then the covariance matrix of the values  $T_j$  are computed for the locations specified  
285 in  $S$  using equation (3.13) (see points 5 and 6 in Figure 2). We also define the  
286 covariance matrices related to a subset  $\mathcal{A}$  such that:

$$(3.21) \quad \Sigma_{i\mathcal{A}} = \begin{bmatrix} \Sigma_{i1} & 0 & 0 & \dots \\ 0 & \Sigma_{i2} & 0 & \dots \\ \vdots & \ddots & \ddots & \vdots \\ \dots & 0 & 0 & \Sigma_{ik} \end{bmatrix}$$

287 where  $\Sigma_{ij}$  is defined in equation (3.13) and  $k = |\mathcal{A}|$ .  $\Sigma_{i\mathcal{A}}$  is used in the final step of  
 288 Algorithm 1 which maximise the mutual information (see points 7 and 8 in Figure 2),  
 289 as described in Algorithm 2, where  $H$  is the conditional entropy function defined as  
 290 (see [5]):

$$(3.22) \quad H(i|\mathcal{A}) = \frac{1}{2} \log \Sigma_{i\mathcal{A}}^2 + \frac{1}{2} (\log(2\pi) + 1)$$

291 and where  $\delta_i$  denotes the mutual information parameter [5]:

$$(3.23) \quad \delta_i = \frac{\Sigma_{ii}^2 - \Sigma_{i\mathcal{A}} \Sigma_{\mathcal{A}\mathcal{A}}^{-1} \Sigma_{\mathcal{A}i}}{\Sigma_{ii}^2 - \Sigma_{i\bar{\mathcal{A}}} \Sigma_{\bar{\mathcal{A}}\bar{\mathcal{A}}}^{-1} \Sigma_{\bar{\mathcal{A}}i}}$$

---

**Algorithm 2:** Maximise Mutual Information (MI) using lazy evaluations.

---

**Input:** Covariance matrix  $\Sigma_{ij}$ , number of sensors  $k$ , set of coordinates  $\mathcal{S}$

```

1  $\mathcal{A} \leftarrow \emptyset$ 
2 foreach  $i \in \mathcal{S}$  do
3    $\delta_i \leftarrow +\infty$ 
4 for  $j=1$  to  $k$  do
5   foreach  $i \in \bar{\mathcal{A}} = \mathcal{S} \setminus \mathcal{A}$  do
6      $current_i \leftarrow false$ 
7     while  $current_i == true$  do
8        $i^* \leftarrow \operatorname{argmax}_{i \in \mathcal{S} \setminus \mathcal{A}} \delta_i$ 
9       if  $current_{i^*} == true$  then
10        break
11        Compute  $\Sigma_{i\mathcal{A}}$  ▷ using equation (3.21) for  $i$  and  $\mathcal{A}$ 
12        Compute  $\Sigma_{i\bar{\mathcal{A}}}$  ▷ using equation (3.21) for  $i$  and  $\bar{\mathcal{A}}$ 
13         $\delta_{i^*} \leftarrow H(i|\mathcal{A}) - H(i|\bar{\mathcal{A}})$  ▷ with  $H$  defined in (3.22)
14         $current_{i^*} \leftarrow true$ 
15    $\mathcal{A} \leftarrow \mathcal{A} \cup i^*$ 
16 return  $\mathcal{A}$ 

```

---

292 We developed a MCMC based wrapper that works with a smaller grid of points  
 293  $\mathcal{S}$ , then identifies the vertices of the grid  $\mathcal{A}$  that are potential frontiers to be ex-  
 294 plored further. These optimal coordinates in  $\mathcal{S}$  are thus adjusted. If the adjustment  
 295 has improved the overall mutual information we keep the modification. Using this  
 296 technique we iteratively adjust  $\mathcal{S}$  until the mutual information value converges.

297 **3.4. Implementation.** A code implementing Algorithm 1 and Algorithm 2 us-  
 298 ing TensorFlow.1.4 [28] is available at [https://github.com/roxarcucci/VGPosp.](https://github.com/roxarcucci/VGPosp.git)  
 299 [git](https://github.com/roxarcucci/VGPosp.git). Instructions for running the tests and algorithms are described in the file  
 300 README.md. The algorithms were initially implemented in Python and reimple-  
 301 mented later in TensorFlow in order to further improve the efficiency of the run-time  
 302 through multi-threaded, parallelised execution and automatic scalability to more  
 303 computational cores. Our implemented model is represented in the form of a com-  
 304 putational data-flow graph that is instantiated once a session object is defined. The  
 305 built-in TensorFlow compiler identifies all dependencies within our algorithms and  
 306 assigns multi-threaded computational tasks to our resources. TensorBoard creates  
 307 a visual representation of the nodes and connections, it enables the developer to  
 308 debug connectivity errors. The Scalars tool that allows the tracking of any metric of  
 309 interest during model training or optimisation was also used.

#### 310 4. RESULTS AND DISCUSSIONS

311 In this section, two test cases are used to discuss our Variation Gaussian Process for  
 312 optimal sensor placement (VGPosp):

- 313 • The first test case, named the sine model, is a simplified two-dimensional  
 314 model of a sine function to test the efficiency, accuracy and precision of VGP  
 315 compared to GP. The comparison between GP and VGP is done only for  
 316 the sine model as the complexity of GP is too high to be trained for a real  
 317 test case.
- 318 • The second test case is a real three-dimensional test case considering a room  
 319 within the Clarence Centre building located in Elephant and Castle, Lon-  
 320 don, UK. In this test case, the predictive model is the Computational Fluid  
 321 Dynamics (CFD) software Fluidity. Optimal sensors location is proposed.  
 322 The benefit of using sensors optimally located is proved by showing how the  
 323 predictive model error can be more efficiently reduced by using Data Assim-  
 324 ilation technology.

325 **4.1. Test case 1: Sine model.** This section aims to compare the efficiency, the  
 326 accuracy and the precision of GP and VGP. The test sine function used is defined  
 327 in equation(4.1).

$$(4.1) \quad f(x, y) = \sin\left(\frac{2}{3}\pi x\right) + \sin\left(\frac{2}{3}\pi y\right)$$

328 In order to prove that VGP is more efficient than a GP approach, the training time  
 329 as a function of the number of training points for both method are shown in Figure 3.

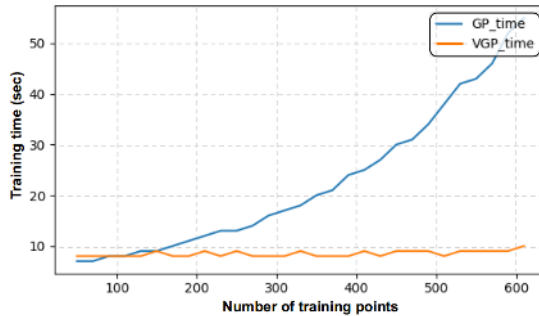


FIGURE 3. Training time as a function of number of training points when using a Gaussian Process (GP) or a Variation Gaussian Process (VGP).

330 Up to 150 number of training points, the GP and the VGP method both take a little  
 331 bit less than 10 sec to be trained. However, when using more training points, i.e.  
 332 more than 150 number of points, the training time of the GP increases drastically,  
 333 while the VGP training time stays constant, around 10 sec, independently of the  
 334 number of points. For example, when considering 600 training points, the training  
 335 time is divided by 5.5 when using the VGP approach.

336 The accuracy  $e$  and the root mean squared error (also called precision),  $RMSE$  of  
 337 the model  $\mathcal{M}$  are:

$$(4.2) \quad e_{\mathcal{M}}(N) = \sum_{i=1}^N |f_{True}(x_i, y_i) - f_{\mathcal{M}}(x_i, y_i)|$$

338 where  $N$  is the number of training points, and

$$(4.3) \quad RMSE_{\mathcal{M}}(N) = \sqrt{\frac{\|F_{\mathcal{M}} - F_{True}\|_{L^2}}{\|F_{True}\|_{L^2}}}$$

339 where  $F_{\mathcal{M}}$  and  $F_{True}$  denote the vectors  $F_{\mathcal{M}} = [f_{\mathcal{M}}(x_1, y_1), \dots, f_{\mathcal{M}}(x_N, y_N)]$  and  
 340  $F_{True} = [f_{True}(x_1, y_1), \dots, f_{True}(x_N, y_N)]$ , the *True* model denotes the function in equa-  
 341 tion (4.1) and the model  $\mathcal{M}$  stands for GP or VGP.

342 The accuracy (equation (4.2)) and the precision (equation (4.3)) of the two models  
 343 as a function of the number of training points are shown in Figure 4. From Figure 4a,  
 344 when using less than 150 training points, the two models highlight the worst accuracy,  
 345 i.e. the highest values. When using more than 150 number of training points, it can  
 346 be seen that the accuracy of GP is lower than 0.03, while the VGP accuracy is lower



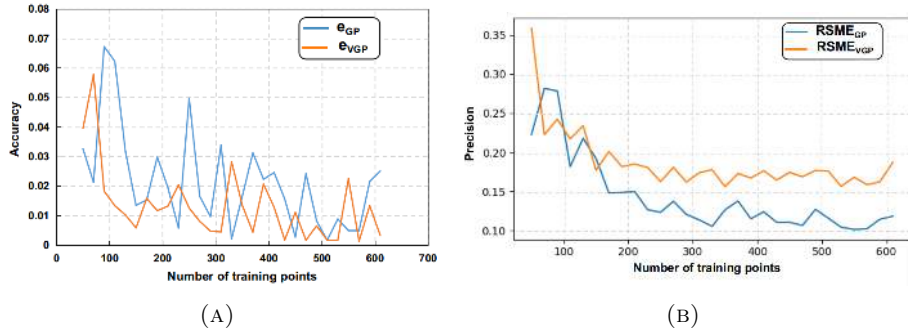


FIGURE 4. (A) Accuracy  $e$  and (B) Precision  $RMSE$  as a function of number of training points when using a Gaussian Process (GP) and a Variation Gaussian Process (VGP).

347 than 0.02. Globally, the VGP method is slightly more accurate than GP even if the  
 348 accuracy can be considered as the same order of magnitude. However, looking at  
 349 Figure 4b, the GP model is more precise than the VGP. For both model, the RMSE  
 350 is relatively high when using less than 200 number of training points. When using  
 351 more training points, the RMSE reaches a plateau with values for the GP and VGP  
 352 model of about 0.12 and 0.17, respectively.

353 Overall, it has been shown that the VGP method is a good trade-off between the  
 354 efficiency, the accuracy and the precision and will then be used as such an assumed  
 355 tool in the second test case.

#### 356 4.2. Test case 2: Real test case.

357 4.2.1. *Predictive model: Computational Fluid Dynamics simulation using Fluidity*  
 358 *software.* The simulated data used to train our VGPosp is obtained using Fluidity, a  
 359 parallel open-source CFD software (<http://fluidityproject.github.io/>). It uses  
 360 finite elements to solve the following incompressible three dimensional Navier-Stokes  
 361 equations, continuity equation (4.4) and momentum equation (4.5), on unstructured  
 362 grids [35]:

$$(4.4) \quad \nabla \cdot \bar{u} = 0$$

363

$$(4.5) \quad \frac{\partial \bar{u}}{\partial t} + \bar{u} \cdot \nabla \bar{u} = -\frac{1}{\rho} \nabla \bar{p} + \nabla \cdot [(\nu + \nu_\tau) \nabla \bar{u}]$$

364 where  $\bar{u}$  is the resolved velocity (m/s),  $\bar{p}$  is the resolved pressure (Pa),  $\rho$  is the fluid  
 365 density (kg/m<sup>3</sup>),  $\nu$  is the kinematic viscosity (m<sup>2</sup>/s) and  $\nu_\tau$  is the anisotropic eddy

366 viscosity ( $\text{m}^2/\text{s}$ ).

367 Turbulence is resolved using Large Eddy Simulation (LES), where the eddies smaller  
368 than a scale  $\Delta$  are parametrised using a subgrid-scale module, while the larger eddies  
369 are fully resolved. The subgrid-scale model in Fluidity is based on the Smagorinsky  
370 model [36, 37].

371 The transport of a scalar field  $C$  (i.e, a passive tracer or pollutant concentration) in  
372  $\text{kg}/\text{m}^3$  is expressed using the advection-diffusion equation (4.6):

$$(4.6) \quad \frac{\partial C}{\partial t} + \nabla \cdot (\mathbf{u}C) = \nabla \cdot (\overline{\kappa_C} \nabla C) + F$$

373 where  $\mathbf{u}$  is the velocity vector ( $\text{m}/\text{s}$ ),  $\overline{\kappa_C}$  is the diffusivity tensor of the pollutant in  
374 an excess of air ( $\text{m}^2/\text{s}$ ) and  $F$  represents the source terms ( $\text{kg}/\text{m}^3/\text{s}$ ).

375 The temperature field  $T$  (Kelvin) is expressed using equation (4.7):

$$(4.7) \quad \frac{\partial T}{\partial t} + \nabla \cdot (\mathbf{u}T) = \nabla \cdot (\overline{\kappa_T} \nabla T) + \frac{Q}{\rho c_p}$$

376 where  $\mathbf{u}$  is the velocity vector ( $\text{m}/\text{s}$ ),  $\overline{\kappa_T}$  is the thermal diffusivity tensor ( $\text{m}^2/\text{s}$ ),  $Q$   
377 represents thermal source terms ( $\text{W}/\text{m}^3$ ),  $\rho$  is the fluid density ( $\text{kg}/\text{m}^3$ ) and  $c_p$  is the  
378 fluid specific heat capacity ( $\text{J}/\text{kg}/\text{K}$ ). The behaviour of the atmospheric boundary  
379 layer in Fluidity is represented using a turbulent inlet velocity based on a synthetic  
380 eddy method [38, 39]. Fluidity uses mesh adaptivity where the mesh can be dynam-  
381 ically refined, during the simulation, in areas of physical significance to the user [40].

382 *4.2.2. Test case set up description.* The test case considered in this paper is a  
383 room within the Clarence Centre building located at London South Bank Uni-  
384 versity (LSBU) near Elephant and Castle in London, UK (Figure 5). The test  
385 room has three windows depicting in blue in Figure 5. This test site was used  
386 to conduct a one-day field study in January 2018 with the MAGIC project (<http://www.magic-air.uk/>, [41]) during which 7 sensors were monitoring the indoor tem-  
387 perature and  $\text{CO}_2$  concentration. The CFD simulation performed in this paper aims  
388 to replicate a cross ventilation scenario, where the test room windows on both sides  
389 of the building were opened.  
390

391 As shown in Figure 6, the computational domain considered to do the numerical  
392 simulations includes the entire Clarence building and the test room, as well as the  
393 immediate building upwind in order to replicate the local flow conditions near the  
394 windows. The mesh is defined such that the resolution is increased in the room  
395 (setting the grid edge length to 0.1 m) and particularly at the openings (grid edge  
396 length set to 0.02 m). It progressively decreases in the overall domain to reach an

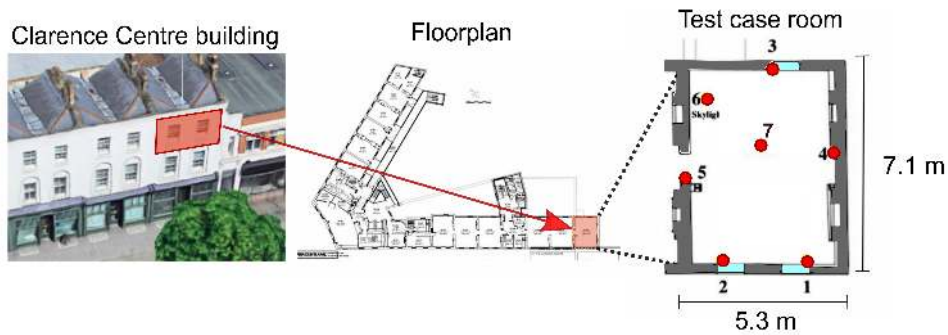


FIGURE 5. The test case room is located in Clarence Centre building in London, UK. The red dots denotes the location of sensors during a field experiment and blue rectangles shows the location of the three windows.

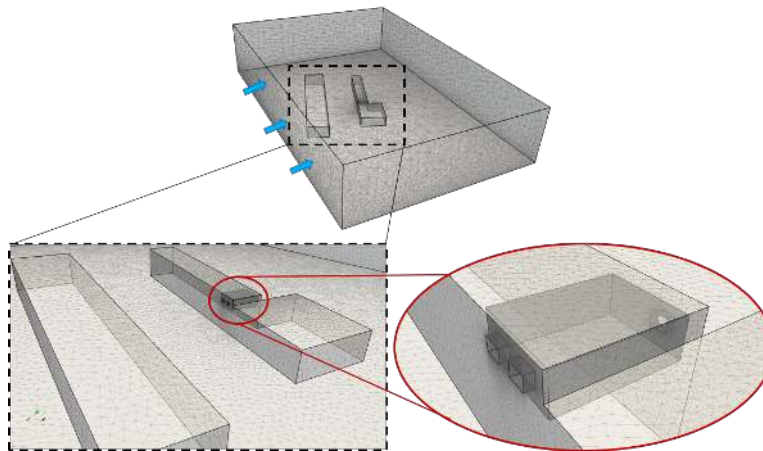


FIGURE 6. Computational domain and surface mesh of the area of interest showing the Clarence Centre and the upwind building as well as the test case room. The blue arrows denote the wind direction.

397 edge length of 10 m away from the room as shown in Figure 6, which gives an overall  
 398 number of 285,700 cells, i.e. grid points, in the mesh. The total number of nodes  
 399 within the room is about  $1.5 \times 10^5$ .

400 The boundary conditions are set to replicate the experimental conditions. A log-law  
 401 turbulent inlet velocity is imposed upwind, corresponding to a wind direction of  $201^\circ$ .  
 402 It is parametrised with an incoming wind velocity of 2.58 m/s at 28.5 m. No slip

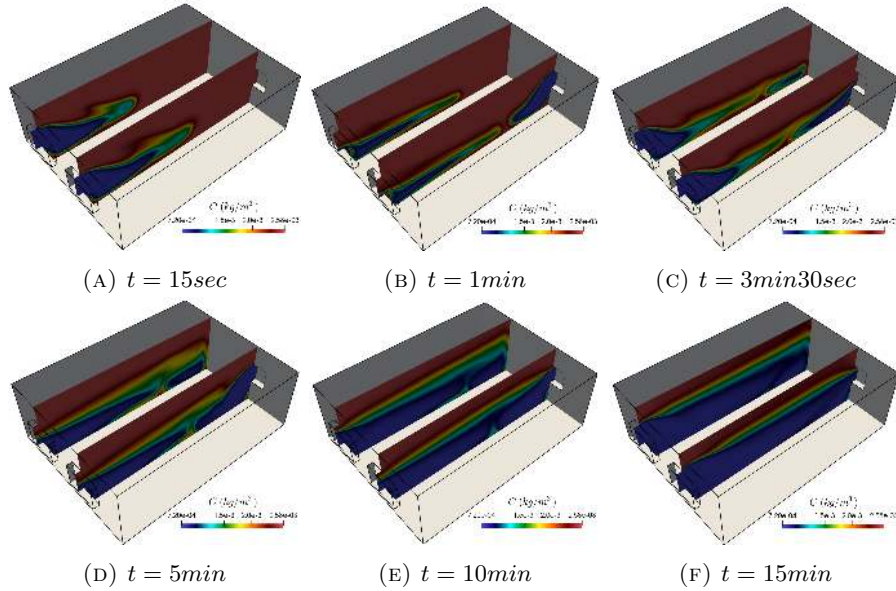


FIGURE 7. Concentration field of  $CO_2$  on two vertical slices in the room at different time. The scale is between  $7.2 \times 10^{-4} kg/m^3$  (blue colour) and  $2.58 \times 10^{-3} kg/m^3$  (red colour).

403 boundary conditions are imposed at the bottom of the domain and on the walls of  
 404 the test room. The initial temperature is set to 19.5 °C inside the room and 9.1  
 405 °C outside. Before opening the windows, based on sensors data, the average  $CO_2$   
 406 concentration in the room is set to  $2.58 \times 10^{-3} kg/m^3$  (1420 ppm) while  $7.2 \times 10^{-4}$   
 407  $kg/m^3$  (400 ppm), is prescribed outside as a background pollution level.

408 The simulation was run in parallel on 20 CPU and for an overall simulation time  
 409 of 15 min, leading to about 3500 timesteps. In this paper, the target variables is  
 410 the concentration  $C$  of  $CO_2$  within the room. As an example, the evolution of the  
 411 concentration field on different planes in the room within the room at different times  
 412 are shown in Figure 7 and Figure 8. At the beginning of the simulation, the outdoor  
 413 air enters the room gradually and concentration stratification starts to occur after  
 414 2 minutes 30 seconds. It can be seen that the concentration in the room starts to  
 415 reach a steady state after 5 minutes and does not change anymore after 15 minutes  
 416 of simulations.

417 4.2.3. *Results.* The training set consists in 10,000 points, exceeding the amount used  
 418 in previous work by a factor of 150 [4, 5]. The quantity and 3D spatial positioning of

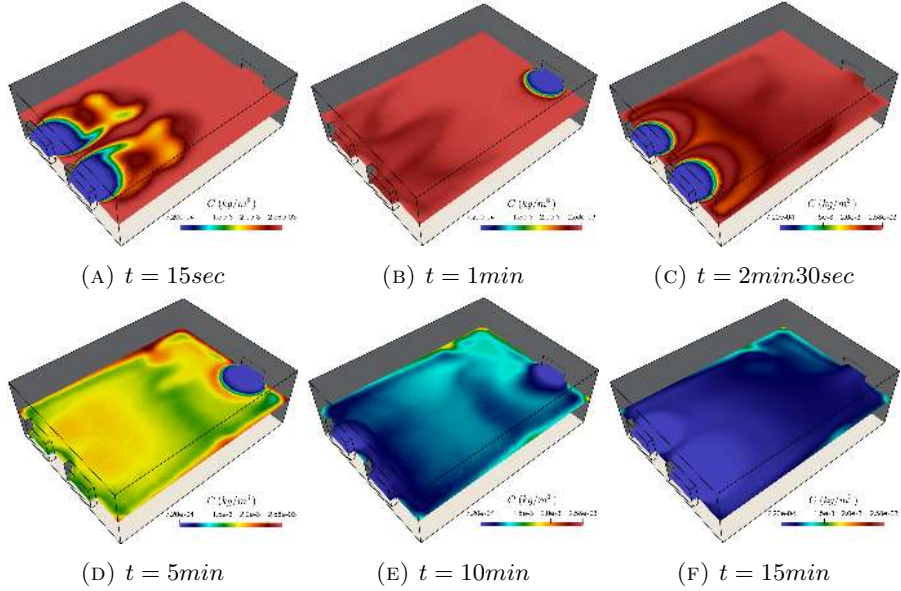


FIGURE 8. Concentration field of  $CO_2$  on an horizontal plane in the room at different time. The scale is between  $7.2 \times 10^{-4} kg/m^3$  (blue colour) and  $2.58 \times 10^{-3} kg/m^3$  (red colour).

419 the training set was sufficient to capture the phenomenology of the indoor environ-  
 420 nment. The CFD results used to train the VGP are taken between 2 min 30 sec and 5  
 421 min, period during which the stratification of the concentration is established. The  
 422 solution of this dynamical system  $X$  in (3.1) includes the physical variables  $[P, T, C]$ ,  
 423 where  $P$  is the pressure,  $T$  the temperature and  $C$ , the physical variables target, the  
 424  $CO_2$  concentration.

425 The simulated training data had features with non-Gaussian likelihoods, causing  
 426 potential problems for spatial learning with Gaussian Processes. While the use of a  
 427 Variational Gaussian Process helps overcome this issue, we further generalised our  
 428 training data through the use of a Masked Autoregressive Flow model that transforms  
 429 the likelihoods of the input features to the family of Gaussian-distributions.

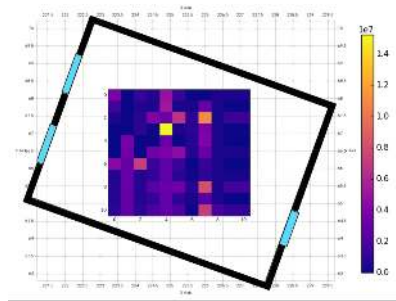
430 The results of the optimal sensor placement are discussed in the following. Firstly,  
 431 the scalability issues related to dense grid initialisations of set  $S$  are addressed.  
 432 Secondly, the introduction of the MCMC based fine-tuning algorithm is motivated.  
 433 Finally, the optimal sensor placement solutions provided by our proposed VGPosp  
 434 model are presented.

435 The placement Algorithm 2 is executed on a predefined area of interest, in which a  
 436 density parameter specifies the grid initialisation that defines set  $S$ . Figure 9 demon-  
 437 strates the internal state, i.e. mutual information parameter, of the placement algo-  
 438 rithm before making a selection. For each coordinate  $\delta_i$  is computed (Algorithm 2)  
 439 and the most optimal coordinate is selected into the final selection set  $\mathcal{A}$ . For exam-  
 440 ple, in Figure 9a, the first sensor will be chosen to be located where  $\delta_i$  is the highest,  
 441 i.e. yellow colour part. From Figure 9, it can be seen that the scale of  $\delta_i$  is not  
 442 the same in each sub-figures and becomes narrower. Indeed, the contributions made  
 443 by earlier selections are higher, explaining why the  $\delta_i$  quantities decrease after more  
 444 sensors are added to set  $S$ .

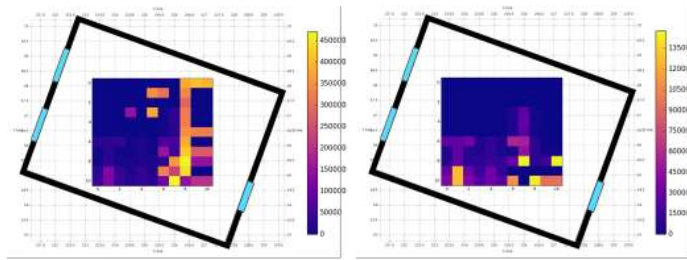
445 The running-times shown in Figure 10 are descriptive of the exponential computa-  
 446 tional cost that is incurred from selecting a larger input set of  $S$ . However, it cannot  
 447 be expected from the selection Algorithm 1 to find the optimal locations in contin-  
 448 uous space when defining only distant, discrete points. In order to reduce the time  
 449 complexity of discovering optimal coordinates in continuous space, we proposed an  
 450 MCMC-based fine-tuning method of set  $S$ . The impact of this procedure is demon-  
 451 strated by Figure 11, where the percentage increase in the optimisation criterion,  
 452 mutual information parameter can be multiple orders of magnitude larger than that  
 453 of the uniform grid instantiation, which may miss more optimal regions. For example  
 454 in the case of a  $7 \times 7 \times 1$  grid instantiation, the fine-tuning Algorithm 1 can achieve a  
 455 3 order of magnitude improvement in the overall mutual information, associated with  
 456 our final selection set  $\mathcal{A}$ . This improvement is achieved after 15 grid optimisation  
 457 attempts. In Figure 12, a  $6 \times 6 \times 4$  grid is considered associated with 40 grid opti-  
 458 misation attempts for each selection. The optimal selection of 7 sensors are plotted  
 459 with crosses as well as all modified grid positions that had achieved improved mutual  
 460 information parameter values. Their colour corresponds with the mutual informa-  
 461 tion parameter that the coordinate had achieved. The final optimal coordinates of  
 462 the room are depicted in Figure 13.

463 Data Assimilation technology is coupled with the predictive model Fluidity. Data  
 464 Assimilation uses observed data from sensors to improve and correct the numer-  
 465 ical results from the simulation. 7 sensors are assimilated in the predictive model.  
 466 The DA algorithm and methodology used was previously successfully coupled with  
 467 Fluidity and is presented in details in [2, 42]. The accuracy of the DA results are  
 468 evaluating using the mean squared error:  $MSE(C) = \frac{\|C - C^{v,n}\|_{L^2}^2}{\|C^{v,n}\|_{L^2}^2}$ , where  $C$  is either  
 469  $C^n$  the Fluidity concentration at time step  $n$  or  $C^{DA}$  the corrected concentration  
 470 using DA and  $C^{v,n}$  is the control variable, i.e. the true observed data. The  $MSE$   
 471 is computed using the 7 optimal sensor locations shown in Figure 13 and compared



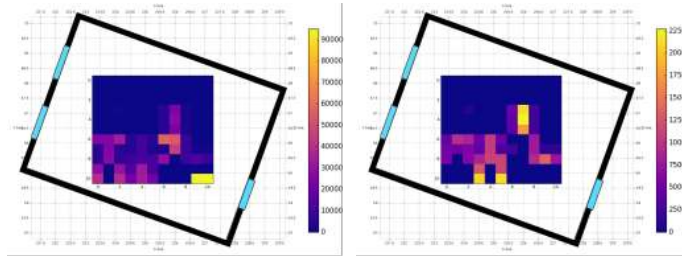


(A) Sensor 1



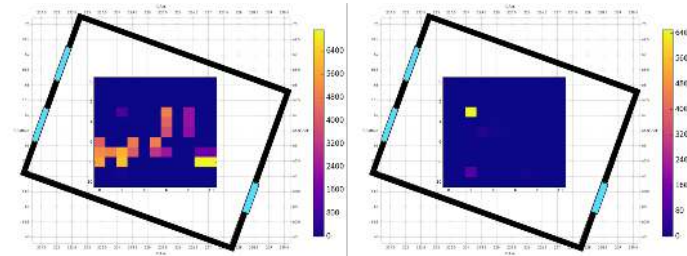
(B) Sensor 2

(C) Sensor 3



(D) Sensor 4

(E) Sensor 5



(F) Sensor 6

(G) Sensor 7

FIGURE 9. Mutual Information parameter  $\delta_i$  on  $M$  grid points ( $11 \times 11 \times 1$ ) for  $k = 7$  sensors. The colours show the value of  $\delta_i$  and the scale is different on each sub-figures. Yellow and violet colours denote high and low  $\delta_i$  values respectively.

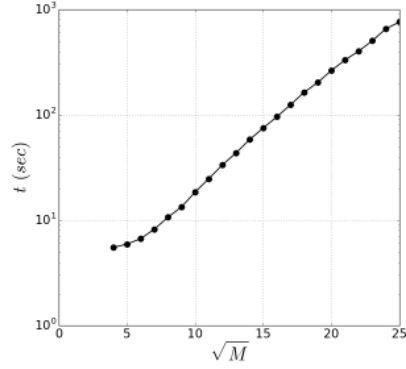


FIGURE 10. Execution time  $t$  of Algorithm 1 as a function of the number of initial grid points  $M$ . The  $y$ -axis is logarithmic.

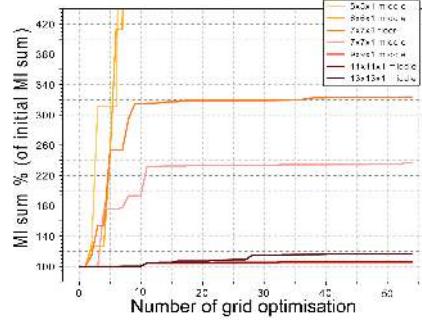


FIGURE 11. Percentage increase in mutual information parameter after the fine-tuning Algorithm 1.

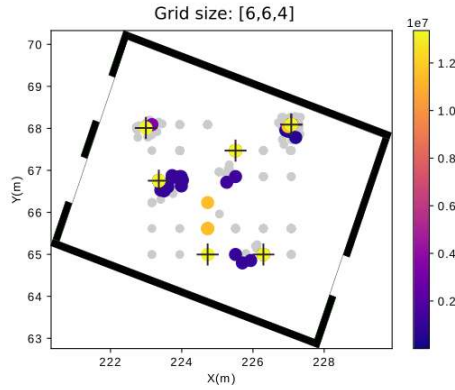


FIGURE 12. Fine-tuning of grid-points and final selection coordinates. Colour represents mutual information parameter of placement. The colour of the point shows the value of the Mutual Information. The crosses depict the final optimal sensor locations.

472 with the  $MSE$  obtained using 7 sensors located randomly. 2000 random sensors  
 473 positioning were performed. Assimilating the seven optimally positioned sensors,  
 474 the error of the predictive model, i.e. Fluidity, is reduced by up to three order of  
 475 magnitude:  $MSE(C^n) = 0.17$  and  $MSE(C^{DA}) = 0.0005$ . Moreover, this error is



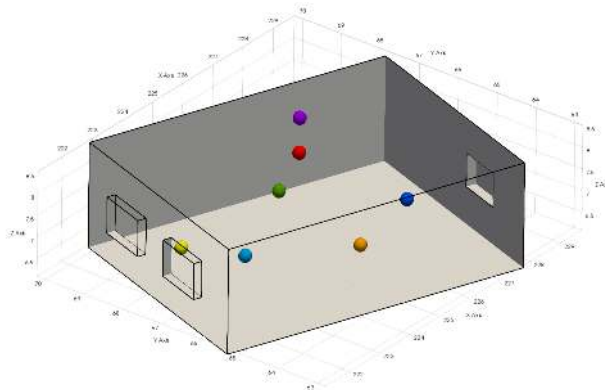


FIGURE 13. Optimal final location of seven sensors in the room of Clarence Centre obtained using the Variational Gaussian Process optimal sensor placement VGPosp in Algorithm 1.

476 up to two order of magnitude lower than the ones computed using random sensors  
 477 placement. In one of the worst random case scenario:  $MSE(C^{DA}) = 0.023$ .

478

## 5. CONCLUSION

479 This work described a novel pipeline for sensor placement, incorporating a Masked  
 480 Autoregressive Flows (MAF) [20] for preconditioning, a Variational Gaussian Process  
 481 (VGP) [14, 15] spatial model and a mutual information-based placement algorithm  
 482 [5]. In this paper, the alterations to the existing placement pipelines are significant  
 483 as they introduce multiple layers of approximations in order to reduce time complex-  
 484 ities. More specifically, VGP was introduced for the sensor placement pipeline to  
 485 tackle the  $O(N^3)$  complexity associated with traditional GP for spatial modelling.  
 486 Increased model generalisation was achieved with MAF that learn non-linear in-  
 487 vertible transformations between complicated transformations and the more flexible  
 488 Normal distribution. All models and algorithms were implemented as a TensorFlow  
 489 computational graph to further reduce run-times as opportunities for parallel compu-  
 490 tation are automatically recognised by the graph compiler. Furthermore, this work  
 491 proposed and developed two extension algorithms. One focused on incorporating  
 492 information and sampling environmental features from the time-series for computing  
 493 mutual information. Secondly, a wrapper algorithm was built to iteratively sub-  
 494 sampling and globally optimise the instantiated set of base grid-coordinates, leading  
 495 to a three-fold increase in mutual information associated with the final selection. The  
 496 combination of these two algorithms achieved stability and a global improvement in  
 497 the selection coordinates.

499 This work is supported by the EPSRC Grand Challenge grant Managing Air for  
 500 Green Inner Cities (MAGIC) EP/N010221/1 and by the EPSRC Centre for Mathe-  
 501 matics of Precision Healthcare EP/N0145291/1

## REFERENCES

- 503 [1] Kelly Frank J. and Fussell Julia C. Improving indoor air quality, health and performance within  
 504 environments where people live, travel, learn and work. *Atmospheric Environment*, 200:90–109,  
 505 2019.
- 506 [2] Rossella Arcucci, Laetitia Mottet, Christopher Pain, and Yi-Ke Guo. Optimal reduced space  
 507 for variational data assimilation. *Journal of Computational Physics*, 379:51–69, 2019.
- 508 [3] L D’Amore, R Arcucci, L Marcellino, and A Murli. A parallel three-dimensional variational  
 509 data assimilation scheme. In *AIP Conference Proceedings*, volume 1389, pages 1829–1831. AIP,  
 510 2011.
- 511 [4] Carlos Guestrin, Andreas Krause, and Ajit Paul Singh. Near-optimal sensor placements in  
 512 gaussian processes. In *Proceedings of the 22nd international conference on Machine learning*,  
 513 pages 265–272. ACM, 2005.
- 514 [5] Andreas Krause, Ajit Singh, and Carlos Guestrin. Near-optimal sensor placements in gaussian  
 515 processes: Theory, efficient algorithms and empirical studies. *Journal of Machine Learning*  
 516 *Research*, 9(Feb):235–284, 2008.
- 517 [6] Rossella Arcucci, Luisa D’Amore, Jenny Pistoia, Ralf Toumi, and Almerico Murli. On the vari-  
 518 ational data assimilation problem solving and sensitivity analysis. *Journal of Computational*  
 519 *Physics*, 335:311–326, 2017.
- 520 [7] Héctor González-Banos. A randomized art-gallery algorithm for sensor placement. In *Proceeed-*  
 521 *ings of the seventeenth annual symposium on Computational geometry*, pages 232–240. ACM,  
 522 2001.
- 523 [8] Kumar Abhishek, MP Singh, Saswata Ghosh, and Abhishek Anand. Weather forecasting model  
 524 using artificial neural network. *Procedia Technology*, 4:311–318, 2012.
- 525 [9] Dan Cornford, Ian T. Nabney, and Christopher KI Williams. Adding constrained discontinu-  
 526 ities to gaussian process models of wind fields. In *Advances in Neural Information Processing*  
 527 *Systems*, pages 861–867, 1999.
- 528 [10] Cheng-Chun Lin and Liangzhu Leon Wang. Forecasting simulations of indoor environment  
 529 using data assimilation via an ensemble kalman filter. *Building and Environment*, 64:169–176,  
 530 2013.
- 531 [11] David JC MacKay. Introduction to gaussian processes. *NATO ASI Series F Computer and*  
 532 *Systems Sciences*, 168:133–166, 1998.
- 533 [12] Carl Edward Rasmussen. Gaussian processes in machine learning. In *Summer School on Ma-*  
 534 *chine Learning*, pages 63–71. Springer, 2003.
- 535 [13] Joaquin Quiñonero-Candela and Carl Edward Rasmussen. A unifying view of sparse approx-  
 536 imate gaussian process regression. *Journal of Machine Learning Research*, 6(Dec):1939–1959,  
 537 2005.
- 538 [14] Michalis K. Titsias. Variational model selection for sparse gaussian process regression. *Report*,  
 539 *University of Manchester, UK*, 2009.
- 540 [15] Michalis Titsias. Variational learning of inducing variables in sparse gaussian processes. In  
 541 *Artificial Intelligence and Statistics*, pages 567–574, 2009.
- 542 [16] John Hagan, AR Gillis, and Janet Chan. Explaining official delinquency: A spatial study of  
 543 class, conflict and control. *The sociological quarterly*, 19(3):386–398, 1978.
- 544 [17] James Hensman, Nicolo Fusi, and Neil D. Lawrence. Gaussian processes for big data. *arXiv*  
 545 *preprint arXiv:1309.6835*, 2013.

- 546 [18] Haitao Liu, Yew-Soon Ong, Xiaobo Shen, and Jianfei Cai. When gaussian process meets big  
547 data: A review of scalable gps. *arXiv preprint arXiv:1807.01065*, 2018.
- 548 [19] Diederik P. Kingma and Max Welling. Auto-encoding variational bayes. *arXiv preprint*  
549 *arXiv:1312.6114*, 2013.
- 550 [20] George Papamakarios, Theo Pavlakou, and Iain Murray. Masked autoregressive flow for density  
551 estimation. In *Advances in Neural Information Processing Systems*, pages 2338–2347, 2017.
- 552 [21] Carl Doersch. Tutorial on variational autoencoders. *arXiv preprint arXiv:1606.05908*, 2016.
- 553 [22] Hadley Wickham. *ggplot2: elegant graphics for data analysis*. Springer, 2016.
- 554 [23] Danilo Jimenez Rezende and Shakir Mohamed. Variational inference with normalizing flows.  
555 *arXiv preprint arXiv:1505.05770*, 2015.
- 556 [24] Mathieu Germain, Karol Gregor, Iain Murray, and Hugo Larochelle. Made: Masked autoen-  
557 coder for distribution estimation. In *International Conference on Machine Learning*, pages  
558 881–889, 2015.
- 559 [25] Noel Cressie. Statistics for spatial data. *Terra Nova*, 4(5):613–617, 1992.
- 560 [26] Satish Tadepally Naren Ramakrishnany, Chris Bailey-Kellogg and Varun N. Pandey. Gaus-  
561 sianprocessesfor active dataminingof spatial aggregates. In *SIAM Data Mining*, pages 427–438,  
562 2005.
- 563 [27] Botond Bócsi, Philipp Hennig, Lehel Csató, and Jan Peters. Learning tracking control with  
564 forward models. In *2012 IEEE International Conference on Robotics and Automation*, pages  
565 259–264. IEEE, 2012.
- 566 [28] Martín Abadi, Ashish Agarwal, Paul Barham, Eugene Brevdo, Zhifeng Chen, Craig Citro,  
567 Greg S. Corrado, Andy Davis, Jeffrey Dean, Matthieu Devin, Sanjay Ghemawat, Ian Good-  
568 fellow, Andrew Harp, Geoffrey Irving, Michael Isard, Yangqing Jia, Rafal Jozefowicz, Lukasz  
569 Kaiser, Manjunath Kudlur, Josh Levenberg, Dandelion Mané, Rajat Monga, Sherry Moore,  
570 Derek Murray, Chris Olah, Mike Schuster, Jonathon Shlens, Benoit Steiner, Ilya Sutskever,  
571 Kunal Talwar, Paul Tucker, Vincent Vanhoucke, Vijay Vasudevan, Fernanda Viégas, Oriol  
572 Vinyals, Pete Warden, Martin Wattenberg, Martin Wicke, Yuan Yu, and Xiaoqiang Zheng.  
573 TensorFlow: Large-scale machine learning on heterogeneous systems, 2015. Software available  
574 from tensorflow.org.
- 575 [29] David M. Blei, Alp Kucukelbir, and Jon D. McAuliffe. Variational inference: A review for  
576 statisticians. *Journal of the American Statistical Association*, 112(518):859–877, 2017.
- 577 [30] Solomon Kullback and Richard A. Leibler. On information and sufficiency. *The annals of*  
578 *mathematical statistics*, 22(1):79–86, 1951.
- 579 [31] Ian Goodfellow, Yoshua Bengio, and Aaron Courville. *Deep learning*. MIT press, 2016.
- 580 [32] Viet Hung Tran. Copula variational bayes inference via information geometry. *arXiv preprint*  
581 *arXiv:1803.10998*, 2018.
- 582 [33] Matthew James Beal et al. *Variational algorithms for approximate Bayesian inference*. Uni-  
583 versity of London, 2003.
- 584 [34] Dustin Tran, Rajesh Ranganath, and David M Blei. The variational gaussian process. *arXiv*  
585 *preprint arXiv:1511.06499*, 2015.
- 586 [35] AMCG. Fluidity manual (Version 4.1), 2015.
- 587 [36] J. Smagorinsky. General Circulation Experiments With the Primitive Equations. *Monthly*  
588 *Weather Review*, 91(3):99–164, 1963.
- 589 [37] T. Bentham. *Microscale modelling of air flow and pollutant dispersion in the urban environ-*  
590 *ment*. PhD thesis, Imperial College London, 2004.
- 591 [38] D. Pavlidis, G.J. Gorman, J.L.M.A. Gomes, C. Pain, and H. ApSimon. Synthetic-Eddy Method  
592 for Urban Atmospheric Flow Modelling. *Boundary-Layer Meteorology*, 136:285–299, 2010.
- 593 [39] N. Jarrin, S. Benhamadouche, D. Laurence, and R. Prosser. A synthetic-eddy-method for  
594 generating inflow conditions for large-eddy simulations. *International Journal of Heat and*  
595 *Fluid Flow*, 27(4), 2006.
- 596 [40] Christopher Pain, A. P. Uempleby, C. R.E. de Oliveira, and A. J.H. Goddard. Tetrahedral  
597 mesh optimisation and adaptivity for steady-state and transient finite element calculations.  
598 *Computer Methods in Applied Mechanics and Engineering*, 190(29-30):3771–3796, 2001.

- 599 [41] Jiyun Song, S. Fan, William Lin, L. Mottet, H. Woodward, M. Davies Wykes, R. Arcucci,  
600 D. Xiao, J-E Debay, H. ApSimon, et al. Natural ventilation in cities: the implications of fluid  
601 mechanics. *Building Research & Information*, 46(8):809–828, 2018.
- 602 [42] E. Aristodemou, R. Arcucci, L. Mottet, A. Robins, C. Pain, and Y.-K. Guo. Enhancing CFD-  
603 LES air pollution prediction accuracy using data assimilation. *Building and Environment*,  
604 165:106383, 2019.

605 ACCRONYMS

- 606 **CFD:** Computational Fluid Dynamics
- 607 **DA:** Data Assimilation
- 608 **ELBO:** Evidence Lower Bound
- 609 **GP:** Gaussian Process
- 610 **IAQ:** Indoor Air Quality
- 611 **KL:** Kullback-Leibler
- 612 **LES:** Large Eddy Simulation
- 613 **LSBU:** London South Bank University
- 614 **MADE:** Masked Autoencoder for Distribution Estimation
- 615 **MAF:** Masked Autoregressive Flows
- 616 **MCMC:** Markov-Chain Monte Carlo
- 617 **MI:** Mutual Information
- 618 **SGP:** Sparse Variational Process
- 619 **VGP:** Variational Gaussian Process
- 620 **VGPosp:** Variational Gaussian Process optimal sensor placement

621 *Authors addresses:* Gabor Tajnafoi, Data Science Institute, Dept. of Computing, Im-  
622 perial College London, UK, e-mail: gabor.tajnafoi18@imperial.ac.uk. Rossella Ar-  
623 cucci, Data Science Institute, Dept. of Computing, Imperial College London, UK, e-mail:  
624 r.arcucci@imperial.ac.uk. Laetitia Mottet, Dept. of Earth Science & Engineering, Impe-  
625 rial College London, UK, e-mail: l.mottet@imperial.ac.uk. Carolanne Vouriot, Dept. of  
626 Civil Engineering, Imperial College London, UK, e-mail: carolanne.vouriot12@imperial.ac.uk.  
627 Miguel Molina-Solana, Dept. of Computer Science and AI, Universidad de Granada,  
628 Spain, e-mail: miguelmolina@ugr.es. Christopher Pain, Dept. of Earth Science & En-  
629 gineering, Imperial College London, UK, e-mail: c.pain@imperial.ac.uk. Yi-Ke Guo,

630 Data Science Institute, Dept. of Computing, Imperial College London, UK, e-mail:  
631 [y.guo@imperial.ac.uk](mailto:y.guo@imperial.ac.uk).